Title

Lineage specific histories of *Mycobacterium tuberculosis* dispersal in Africa and Eurasia

Author Affiliation

Mary B O'Neill[a,b,*], Abigail Shockey[b], Alex Zarley[c], William Aylward[d], Vegard Eldholm[e], Andrew Kitchen[f], Caitlin S Pepperell[b,g]

[a]Laboratory of Genetics, University of Wisconsin-Madison, Madison, WI 53706, USA
[b]Department of Medical Microbiology and Immunology, University of Wisconsin-Madison, Madison, WI 53706, USA
[c]Department of Geography, University of Wisconsin-Madison, WI 53706, USA
[d]Department of Classical and Ancient Near Eastern Studies, University of Wisconsin-Madison, Madison, WI 53706, USA
[e]Infection Control and Environmental Health, Norwegian Institute of Public Health, 0456 Oslo, Norway
[f]Department of Anthropology, University of Iowa, Iowa City, IA 52242, USA
[g]Department of Medicine, University of Wisconsin-Madison, Madison, WI 53706, USA
*Present address: Unit of Human Evolutionary Genetics, Institut Pasteur, 75015 Paris, France

Corresponding Authors

Caitlin S Pepperell
1550 Linden Drive
5301 Microbial Sciences Building
Madison, WI 53706
(608) 262-5983
cspepper@medicine.wisc.edu

Andrew Kitchen
17 N. Clinton Street
114 Macbride Hall
Iowa City, Iowa 52242
(319) 335-2891
andrew-kitchen@uiowa.edu

Keywords

phylogeography, evolution, pathogen, migration, demography

Abstract

Mycobacterium tuberculosis (*M.tb*) is a globally distributed, obligate pathogen of humans that can be divided into seven clearly defined lineages. Identifying how the ancestral clone of *M.tb* spread and differentiated is important for identifying the ecological drivers of the current pandemic. We reconstructed *M.tb* migration in Africa and Eurasia, and investigated lineage specific patterns of spread. Applying evolutionary rates inferred with ancient *M.tb* genome calibration, we link *M.tb* dispersal to historical phenomena that altered patterns of connectivity throughout Africa and Eurasia: trans-Indian Ocean trade in spices and other goods, the Silk Road and its predecessors, the expansion of the Roman Empire and, the European Age of Exploration. We find that Eastern Africa and Southeast Asia have been critical in the dispersal of *M.tb*. Our results reveal complex relationships between spatial dispersal and expansion of *M.tb* populations, and delineate the independent evolutionary trajectories of bacterial sub-populations underlying the current pandemic.

Introduction

The history of tuberculosis (TB) has been rewritten several times as genetic data accumulate from its causative agent, *Mycobacterium tuberculosis* (*M.tb*). In the nascent genomic era, these data refuted the long-held hypothesis that human-adapted *M.tb* emerged from an animal adapted genetic background represented among extant bacteria by *Mycobacterium bovis*, another member of the *Mycobacterium tuberculosis* complex (MTBC) (Brosch et al. 2002). Genetic data from bacteria infecting multiple species of hosts revealed that currently known non-primate-adapted strains form a nested clade within the diversity of extant *M.tb* (Behr et al. 1999; Brosch et al. 2002; Hershberg et al. 2008).

M.tb can be classified into seven well-differentiated lineages, which differ in their geographic distribution and association with human sub-populations (Hirsh et al. 2004; Gagneux et al. 2006). This observation led to the hypothesis that *M.tb* diversity has been shaped by human migrations out of Africa, and that the most recent common ancestor (MRCA) of extant *M.tb* emerged in Africa approximately 73,000 years ago, coincident with estimated waves of human migration (Comas et al. 2013). Human out of Africa migrations are a plausible means by which *M.tb* could have spread globally. However, several features of *M.tb* population genetics suggest it has diversified over relatively short time scales: for example, the species is characterized by low genetic diversity (Eldholm and Balloux 2016) and high rates of non-synonymous polymorphism (Rocha et al. 2006).

The observation of limited diversity among extant *M.tb* could be reconciled with the out of Africa scenario if *M.tb*'s rate of evolution were orders of magnitude lower than estimates from other bacterial pathogens, or if *M.tb* exhibited dramatic rate decay such that substitution rates varied by several orders of magnitude as a function of temporal sampling window (Comas et al. 2013; Eldholm and Balloux 2016). There are at least nine published estimates of the rate of *M.tb* molecular evolution, which use a variety of calibration methods (Eldholm et al. 2016). Rate estimates calibrated with sampling dates, historical events, experimental infection in non-human primates, recent transmission events, and ancient DNA are concordant. Critically, *M.tb* rate estimates are similar to those of other bacterial species, and are inconsistent with the out of Africa hypothesis. In addition, a recent meta-analysis of evolutionary rate estimates in bacteria noted that 'reliable rate estimates for *M. tuberculosis*, estimated over sampling frames of 15 and 895 years, were nearly identical' (Duchêne et al. 2016), suggesting that *M.tb* is not characterized by the dramatic rate decay that would be needed to reconcile observed data with the out of Africa hypothesis.

When calibrated with ancient DNA, the estimates of the time to most recent common ancestor (TMRCA) for the MTBC are <6,000 years before present (Bos et al. 2014; Kay et al. 2015). This is not necessarily the time period over which TB first emerged, as it is possible – particularly given the apparent absence of recombination among *M.tb* (Pepperell et al. 2013) – that the global population has undergone clonal replacement events that displaced ancient diversity from the species.

M.tb is an obligate pathogen of humans with a global geographic range. The finding of a recent origin for the extant *M.tb* population raises the question of how the organism could have spread within this timeframe to occupy its current distribution. *M.tb* populations in the Americas show the impacts of European colonial movements as well as recent immigration (e.g. Pepperell et al. 2011); the role of other historical phenomena in driving TB dispersal is not well understood. Here we sought to reconstruct the migratory history of *M.tb* populations in Africa and Eurasia within the newly established framework of a recent origin and evolutionary rates derived from ancient DNA data (Bos et al. 2014; Kay et al. 2015). We discovered lineage-specific patterns of migration and a complex relationship between *M.tb* effective population growth and migration. Our results connect *M.tb* migration to major historical events in human history that altered patterns of connectivity in Africa and Eurasia. These findings provide context for a recent

106 evolutionary origin of the MRCA of *M.tb* (Pepperell et al. 2013; Bos et al. 2014; Kay et al. 2015),
107 which represents yet another paradigm shift in our understanding of the history and origin of this
108 successful pathogen.
109
110 Results
111 ***Genetic and geographic structures of global M.tb populations***
112 In order to establish the contemporary geographic distributions of *M.tb* lineages, we translated
113 the spoligotypes reported for 42,358 *M.tb* isolates to their corresponding lineage designations
114 (fig. 1). Geographic patterns in prevalence vary between lineages. Lineage 1 (L1) is prevalent
115 in regions bordering the Indian Ocean, extending from Eastern Africa to Melanesia. Lineage 2
116 (L2) is broadly distributed, with a predominance in Eastern Eurasia and South East Asia.
117 Lineage 3 (L3) is similar to L1 in that its distribution rings the Indian Ocean, but it does not
118 extend into Southeastern Asia, it has a stronger presence in Northern Africa, and a broader
119 distribution across Southern Asia. Lineage 4 (L4) is strikingly well dispersed, with a
120 predominance throughout Africa and Europe and the entire region bordering the Mediterranean.
121 Lineages 5 (L5) and 6 (L6) are found at low frequencies in Western and Northern Africa.
122 Lineage 7 (L7), as previously described (Blouin et al. 2012; Firdessa et al. 2013; Comas et al.
123 2015), is limited to Ethiopia.
124
125 We compiled a diverse collection of *M.tb* genomes for phylogenetic and population genetic
126 inference of the demographic and migratory history of the extant *M.tb* population (*see Methods*).
127 Our dataset consists of whole-genome sequences (WGS) from 552 *M.tb* isolates collected from
128 51 countries (spanning 13 UN geoscheme subregions), which we refer to as the Old World
129 collection (fig. s1, table s1). We included sites in the alignment where at least half of these
130 isolates had confident data (60,787 variant sites; 3,838,249 bp) for subsequent analyses, unless
131 otherwise noted.
132
133 The inferred maximum likelihood phylogeny and Bayesian clustering analysis reveals the well
134 described *M.tb* lineage structure, and some associations are evident between lineages and
135 geographic regions (defined here by the United Nations geoscheme) (fig. s2). The phylogeny
136 has an unbalanced shape, with long internal branches that define the lineages and feathery tips,
137 suggestive of recent population expansion.
138

Genetic diversity, as measured by the numbers of segregating sites and pairwise differences (Watterson's □ and π), varied among lineages (table 1). L1 and L4 group together and have the highest diversity; L2, L3, L5, and L6 have similar levels of diversity and form the middle grouping; L7 has the lowest diversity. We used an analysis of molecular variance (AMOVA) to delineate the effects of population sub-division on *M.tb* diversity (table 1). The Old World collection was highly structured among UN subregions (21% of variation attributable to between-region comparisons), whereas this structure was less apparent when regions were defined by the botanical contents outlined by the World geographic scheme for recording plant distributions (14%). This is consistent with *M.tb*'s niche as an obligate human pathogen, with bacterial population structure directly shaped by that of its host population (i.e. reflected in UN subregions) rather than climatic and other environmental features (reflected in botanical continent definitions). We obtained similar results when the lineages were considered separately, except for L4, which had little evidence of population structure (4% variation among UN subregions, 2% among botanical continents).

Distinct demographic histories of the M.tb lineages

Bayesian inferred trees vary among lineages (fig. 2), likely reflecting their distinct demographic histories. Branch lengths are relatively even across the phylogenies of L1 and L4, whereas L2 and L3 have a less balanced structure. The long, sparse internal branches and radiating tips of L2 and L3 phylogenies are consistent with an early history during which the effective population size remained small (and diversity was lost to drift), followed by more recent population expansion. L5 has a star-like structure, consistent with rapid population expansion. Jointly inferred Bayesian skyline plot (BSP) reconstructions of effective population sizes over time suggest that lineages 1-6 have undergone expansion (fig. 3 – top panel, fig. S3). We estimate that L2 and L3 underwent abrupt expansion at approximately the same time, whereas expansions of L1 and L4 appeared relatively smooth.

We used the methods implemented in ∂a∂i to reconstruct the demographic histories of each *M.tb* population (i.e. lineage) from its synonymous site frequency spectrum (SFS). As demographic inference with ∂a∂i is sensitive to missing data, loci at which any sequence in the individual lineage alignments had a gap or unknown character were removed for these analyses. Consistent with the BSP analyses performed in BEAST, instantaneous expansion and exponential growth models offered an improved fit to the data in comparison with the constant population size model for each lineage and the entire Old World collection (fig. S4).

Parameter estimates varied widely across runs for the exponential growth model, so we report results only for the instantaneous expansion model (table 1).

Major events in M.tb's migratory history

There was evidence of isolation by distance in the global *M.tb* population, as assessed with a Mantel test of correlations between genetic and geographic distances. We defined geographic distances using three schemes: great circle distances, great circle distances through waypoints of human migration as described in (Ramachandran et al. 2005), and distances along historical trade routes. Waypoints are used to make distance estimates more reflective of presumed human migration patterns (i.e., when calculating between-continent distances, it is generally thought that humans did not pass through large bodies of water, and thus a waypoint is used). To allow comparisons between the schemes, values were centered and standardized (*see Methods*). Values of the Mantel test statistic were similar for great circle distances (r = 0.16) and trade network distances (r = 0.16), with distances through waypoints reflective of human migration patterns having a lower value (r = 0.14, $p = 0.0001$ for all three analyses). In analyses of human genetic data, adjustment of great circle distances with waypoints results in a higher correlation between genetic and geographic distances (Ramachandran et al. 2005). Our Mantel test results therefore do not support a pattern of isolation by distance as expected if out of Africa human migrations were the primary influence on global diversity of extant *M.tb* (Comas et al. 2013).

To further investigate a potential influence of ancient human migration on *M.tb* evolution, we calculated the correlation between *M.tb* genetic diversity (π) within subregions and their average distances from Addis Ababa, a proxy for a possible origin of anatomically modern human expansion out of Africa. Contrary to what is observed for human population diversity (Ramachandran et al. 2005), we did not observe a significant decline in *M.tb* diversity as a function of distance in our Old World collection (adjusted R-squared = -0.1, $p = 0.88$), nor when we included samples from the Americas (adjusted R-squared = 8.9×10^{-4}, $p = 0.34$, fig. S5, table S2).

We used the methods implemented in BEAST to reconstruct the migratory history of the entire Old World *M.tb* collection as well as individual lineages within it, modelling geographic origin of isolates (UN subregion or country) as a discrete trait (fig. 4, figs. S6-S10). Using an evolutionary rate calibrated with 18th century *M.tb* DNA of 5×10^{-8} substitutions/site/year (Kay et

al. 2015), which is similar to the rate inferred with data from 1,000 year old specimens (Bos et al. 2014), our estimate of the time to most recent common ancestor for extant *M.tb* is between 4032 BCE and 2172 BCE (table 1; date ranges are based on the upper and lower limits of the 95% highest posterior density (HPD) for the rate reported in Kay et al. (2015) which is more conservative than the 95% HPD of our model). We infer an African origin for the MRCA (Eastern or Western subregion, table 1, fig. 4, fig. S6). Shortly after emergence of the common ancestor, we infer a migration of the L1-L2-L3-L4-L7 ancestral lineage from Western to Eastern Africa (we estimate prior to 2683 BCE), with subsequent migrations occurring out of Eastern Africa.

In our phylogeographic reconstruction, emergence of L1 follows migration from Eastern Africa to Southern Asia at some time between the 3rd millennium and 4th century BCE (table 1, fig. 4, fig. S6). L1 has an 'out of India' phylogeographic pattern (fig. S7), with diverse Indian lineages interspersed throughout the phylogeny. This suggests that the current distribution of L1 around the Indian Ocean (fig. 1) arose from migrations out of India, from a pool of bacterial lineages that diversified following migration from Eastern Africa.

The phylogeographic reconstruction further indicates that following the divergence of L1, *M.tb* continued to diversify in Eastern Africa, with emergence of L7 there, followed by L4 (table 1, fig. 4, fig. S6). The contemporary distribution of L4 is extremely broad (fig. 1) and in this analysis of the Old World collection we infer an East African location for the internal branches of L4. Notably, in the lineage-specific analyses, we infer a European location for these branches (fig. S7). The difference is likely due to the fact that inference is informed by deeper as well as descendant nodes in the Old World collection. Together, these results imply close ties between Europe and Africa during the early history of this lineage that we estimate emerged in the 1st century CE (368 BCE-362 CE, table 1).

After the emergence of L1 and L7 from Eastern Africa, our analyses suggest that a migration occurring between 697 BCE and 520 CE established L3 in Southern Asia, with subsequent dispersal out of Southern Asia into its present distribution, which includes Eastern Africa (i.e., a back migration of L3 to Africa, fig. 1). We estimate that L2 diversified in South Eastern Asia following migration from Eastern Africa at some point between 697 BCE and 20 BCE (table 1, fig. 4, fig. S6). A previously published analysis of L2 phylogeography also inferred a Southeast Asian origin for the lineage (Luo et al. 2015).

241

242 ***Lineage and region specific patterns of migration***

243 Our phylogeographic reconstruction indicated that temporal trends in migration varied among
244 lineages (fig. 3 – bottom panel). We infer that L1 was characterized by high levels of migration
245 until approximately the 7th century CE, when the rate of migration decreased abruptly and
246 remained stable thereafter. L3, by contrast, exhibited consistently low rates of migration. L2
247 and L4 had more variable trends in migration, as each underwent punctuated increases in
248 migration rate. Temporal trends in growth and migration are congruent for L2 and L4, with
249 increases in migration rate preceding effective population expansions; this is not the case for L1
250 and L3. Taken together, these results suggest that L1 and L3 populations (as well as L5 and
251 L6, fig. S3b) grew *in situ*, whereas range expansion may have contributed to the growth of L2
252 and L4.

253

254 We employed the Bayesian stochastic search variable selection method (BSSVS) in BEAST
255 (Lemey et al. 2009) to estimate relative migration rates within the most parsimonious migration
256 matrix. A map showing inferred patterns of connectivity among UN subregions and relative
257 rates of *M.tb* migration with strong posterior support is shown in fig. 5. South Eastern Asia was
258 the most connected region in our analyses, with significant rates of migration connecting it to
259 eight other regions. Eastern Africa, Eastern Europe, and Southern Asia were also highly
260 connected, with significant rates with six, six, and five other regions, respectively. Western
261 Africa, Eastern Asia, and Western Asia were the least connected regions, with just one
262 significant connection each (to Eastern Africa, South Eastern Asia, and Eastern Europe,
263 respectively). Our sample from Western Asia is, however, limited (table S1) and migration from
264 this region may have consequently been underestimated. The highest rates of migration were
265 seen between Eastern Asia and Southeastern Asia, and between Eastern Africa and Southern
266 Asia.

267

268 Lineage specific analyses suggest that migration between Southern Asia, Eastern Africa, and
269 South Eastern Asia has been important for the dispersal of L1, whereas South Eastern Asia and
270 Eastern Europe have been important for L2 (fig. S11). L3 is similar to L1 in that there is
271 evidence of relatively high rates of migration between Southern Asia and Eastern Africa. There
272 is also evidence of migration within Africa between the eastern and southern subregions. In the
273 analyses of migration for L4, Eastern Africa appeared highly connected with other regions.

274

Phylogeographic reconstruction: limitations and alternatives

These phylogeographic reconstructions are clearly sensitive to sampling, since we cannot identify the roles of unsampled regions in *M.tb*'s migratory history. We maximized geographic diversity in our sample, but were limited by available data and some regions – notably Middle Africa, Northern Africa, and Western Asia – are absent or underrepresented in our sample (fig. S1). Defining the contributions of these undersampled regions to *M.tb*'s migratory history awaits more samples and/or further method development.

De Maio *et al*. (2015) note the sensitivity of discrete trait phylogeographic inference in BEAST to sample selection, as well as overconfidence in the precision of geographic inference, and propose BASTA as an alternative (De Maio et al. 2015). BASTA is sensitive to the choice of prior and we did not have ancillary data to guide the selection of a prior for the Old World migratory history of *M.tb*, precluding its use here. We investigated ∂a∂i as an alternative tool for phylogeographic inference but it did not perform well for this application under conditions of complete linkage of sites (Note S1, fig. S12, fig. S13, table S3, table S4). Lapierre *et al*. (2016) investigated the sensitivity of BEAST inference of demography to sampling regime. They found that the method performed poorly under a 'uniform' sub-sampling regime, in which populations are randomly sampled to the same size (Lapierre et al. 2016). Our results are concordant with Lapierre *et al.* (2016), in that we found inferred migration matrices were not consistent across random sub-samples of our dataset (fig. S14). We also interrogated the relationship between regional sample size and inferred migration rate and did not observe a strong correlation (fig. S14). The phylogeographic inference method implemented here relies on the assumption that sample size reflects deme size (Lemey et al. 2009; De Maio et al. 2015), and within the constraints of available data, we attempted to adjust our sample sizes according the regional prevalence of TB (see *Methods* and fig. S1). According to the classifications proposed by Lapierre *et al*. (2015), our Old World collection represents a 'mixed' sampling scheme (see *Methods*).

We previously demonstrated effects of population expansion, linkage, and purifying selection on *M.tb* genetic diversity (Pepperell et al. 2013). Given these previous observations, we were curious about a potential impact of purifying selection on inference of migration. To address this question, we simulated data under demographic models with and without selection and migration, and then analyzed the resulting sequence alignments in BEAST. Our two population simulation suggests that purifying selection may elevate estimated migration rates, though the

distribution of mean rate estimates for simulations with and without purifying selection broadly overlap (fig. S15). However, analysis of sequence alignments generated under a three population model suggested that selection had a statistically negligible effect on migration rates, which can be observed from plots of the mean relative rates (fig. S16) or of the relative support of migration rates (fig. S17). We note that the discrete migration model implemented in BEAST was able to capture much of the asymmetry of our three population asymmetrical simulations as evidenced by the distribution of relative migration rates and Bayes factor (BF) support for said rates. BEAST also consistently produced similar BF support for rates estimated from data simulated under symmetrical migration models (i.e., those with global $M = 0.5$ or 0.0). Our simulations thus suggest that consistent purifying selection is unlikely to dramatically affect estimates of, or support for, migration rates between populations in these scenarios.

Discussion

Our reconstructions of *M.tb* dispersal throughout the Old World delineate a complex migratory history that varies substantially between bacterial lineages. Patterns of diversity among extant *M.tb* suggest that historical pathogen populations were capable of moving fluidly over vast distances. Using evolutionary rate estimates from ancient DNA calibration, we time the dispersal of *M.tb* to a historical period of exploration, trade, and increased connectivity among regions of the Old World.

Consistent with prior reports (Comas et al. 2013), we infer an origin of *M.tb* on the African continent (table 1, fig. 4, fig. S6). There is a modest preference for Western Africa over Eastern Africa (54% versus 38% inferred probability), likely due to the early branching West African lineages (i.e. *Mycobacterium africanum*, L5 and L6). Larger samples may allow more precise localization of the *M.tb* MRCA, and Northern Africa in particular is under-studied.

We infer L1 to be the first lineage that emerged out of Africa; L1 is currently concentrated in regions bordering the Indian Ocean from Eastern Africa to Melanesia (fig. 1). In our phylogeographic reconstruction, the genesis of this lineage traces to migration from Eastern Africa to Southern Asia at some point between the 3rd millennium and 4th century BCE, with subsequent dispersal occurring out of the Indian subcontinent. Our results suggest that the early history of L1 was characterized by high levels of migration, particularly between Southern Asia and Eastern Africa, and between Southern Asia and South Eastern Asia (fig. 3, fig. S11). The geographic distribution of L1, the timing of its emergence and spread, as well as patterns of

connectivity underlying its dispersal, are all consistent with migration via established trans-Indian Ocean trade routes linking Eastern Africa to Southern and South Eastern Asia (fig. 6). The interval of our timing estimate for the initial migration overlaps with the so-called Middle Asian Interaction sphere in The Age of Integration (2600-1900 BCE), which is marked by increased cultural exchange and trade between civilizations of Egypt, Mesopotamia, the Arabian peninsula, and the Indus Valley (Vogt 1996; Zarins 1996; Parkin and Barnes 2002; Ray 2003; Coningham and Young 2015). East-West contact and trade across the Indian Ocean intensified in the first millennium BCE, when maritime networks expanded to include the eastern Mediterranean, the Red Sea, and the Black Sea (Dilke 1985; Boussac et al. 1995; Ray et al. 1996; Salles 1996). Historical data from the Roman era indicate that crews on trading ships crossing the Indian Ocean comprised fluid assemblages of individuals from diverse regions, brought together under conditions favorable for the transmission of TB (André and Filliozat 1986; Begley and De Puma 1991; Wink 2002; Rauh 2003). These ships would have been an efficient means of spreading *M.tb* among the distant regions involved in trade.

L2 may similarly have an origin in East-West maritime trade across the Indian Ocean, as we infer it arose from a migration event from Eastern Africa to South Eastern Asia during the 1st millennium BCE. In this era, increased sophistication in ship technology allowed for longer voyages (Kent 1979; Blench 1996; Ray et al. 1996; Parkin and Barnes 2002; Wink 2002; Ray 2003). L2 appears to have spread out of Southeast Asia, a highly connected region in our analyses of *M.tb* migration, and is currently found across Eastern Eurasia and throughout South Eastern Asia (fig. 1, fig. 4, fig. S6, fig. S11). Interestingly, although L2 is dominant in Eastern Asia, the region did not appear to have played a prominent role in dispersal of this lineage, except in its exchanges with South Eastern Asia.

In contrast to L1 and L2, L3 appears to have had relatively low rates of migration throughout its history (fig. 3). The contemporary geographic range of L3 is also narrower, extending east from Northern Africa through Western Asia to the Indian subcontinent (fig. 1). A study of lineage prevalence in Ethiopia showed that L3 is currently concentrated in the north of the country (Comas et al. 2015), consistent with our observed north to south gradient in its distribution on the African continent. This is in opposition to L1, which has a southern predominance in Ethiopia and across Eastern Africa (fig. 1). We estimate L3 emerged in Southern Asia ca. 520 CE (177-739 CE). Pakistan harbors diverse strains belonging to L3 (fig. S9), and the Southern Asia region was highly connected with Eastern Africa in our analyses (fig. S11). Trade along

the Silk Road connecting Europe and Asia was very active in the middle of the first millennium, when we estimate L3 emerged (Hansen 2012; Ball 2016); its distribution suggests it spread primarily along trading routes connecting Northeast Africa, Western Asia, and South Asia (André and Filliozat 1986; Sartre 1991; Hansen 2012; Ball 2016) (fig. 6). We speculate that this occurred *via* overland routes, which may have limited the migration of L3 relative to maritime dispersal of the other lineages.

The geographic distribution of L4 is strikingly broad (fig. 1) and it exhibits minimal population structure (table 1). This suggests L4 dispersed efficiently and continued to mix fluidly among regions, a pattern we would expect if it was carried by an exceptionally mobile population of hosts. L4 is currently concentrated in regions bordering the Mediterranean, and elsewhere throughout Africa and Europe (fig. 1). We estimate the MRCA of L4 emerged in the 1st century CE (range 368 BCE-362 CE), during the peak of Roman Imperial power across the entire Mediterranean world and expansionist Roman policies into Africa, Europe, and Mesopotamia (Luttwak 1976; Isaac 2004). The empire reached its greatest territorial extent in the early second century CE, when all of North Africa, from the Atlantic Ocean to the Red Sea, was under a single power, with trade on land and sea facilitated by networks of stone-paved roads and protected maritime routes (Luttwak 1976; Millar 1993; Ball 2016). Primary sources from Roman civilization attest to trade with China, purposeful expeditions for exploration, cartography, and trade in the Red Sea and Indian Ocean (Pfister and Bellinger 1945; Dilke 1985; Begley and De Puma 1991; Erdkamp 2002; Butcher 2003).

We hypothesize that the broad distribution of L4 reflects rapid diffusion from the Mediterranean region along trade routes extending throughout Africa, the Middle East, and on to India, China, and South Eastern Asia. High rates of migration appear to have been maintained for this lineage over much of its evolutionary history (fig. 3); patterns of connectivity implicate Europe and Africa in its dispersal (fig. S11). The association of L4 with European migrants is well described, particularly migrants to the Americas (Gagneux et al. 2006; Pepperell et al. 2011). Here we note bacterial population growth preceded geographic range expansion in L4 ~ca. 15th century (fig. 3), which coincides with the onset of the 'age of exploration' (Alam and Subrahmanyam 2009) that would have provided numerous opportunities for spread of this lineage from Europeans to other populations. We also note the origin and concentration of this lineage on the African continent. Our sample of L4 isolates includes several deeply rooting

African isolates, and African isolates are interspersed throughout the phylogeny (fig. 4, fig. S6, fig. S8).

The migratory histories of L5, L6, and L7 are less complicated than those of lineages 1-4. Specifically, L5 and L6 are restricted to Western Africa and L7 is found only in Ethiopia (fig. 4, fig. S6). The reasons for the restricted distributions of these lineages are not immediately obvious: there is evidence in our analyses that other lineages migrated in and out of Western Africa, and Eastern Africa emerged as highly connected and central to the dispersal of *M.tb* (fig. 5). A potential explanation is restriction of the pathogen population to human sub-populations with distinct patterns of mobility and connectivity that did not facilitate dispersal. This is likely the case for L7, which was discovered only recently (Blouin et al. 2012), and is currently largely restricted to the highlands of northern Ethiopia (Firdessa et al. 2013; Comas et al. 2015). In the case of L6 (also known as *Mycobacterium africanum*), there is evidence suggesting infection is less likely to progress to active disease than for *M. tuberculosis sensu stricto* (Jong et al. 2008), which could have played a role in limiting its dispersal.

Our reconstructions of *M.tb*'s migratory history suggest that patterns of migration were highly dynamic: the pathogen appears to have dispersed efficiently, in complex patterns that nonetheless preserved the distinct structure of each lineage. Some findings, notably inference of population expansion, were consistent across lineages. Though growth of the global *M.tb* population has been described previously (Comas et al. 2013; Pepperell et al. 2013), our results here suggest that the pace and magnitude of expansion, and its apparent relationship to trends in migration, varied among lineages (fig. 3, fig. S3, fig. S11).

Our analyses suggest that the expansion of L2 was preceded by an impressive increase in its rate of migration (fig. 3), implying that growth of the pathogen population was facilitated by expansion into new niches. Our phylogeographic reconstructions implicate Russia, Central Asia, and Western Asia in the recent migratory history of L2 (fig. S10, fig. S11), which is consistent with a published phylogeographic analysis of L2 (Luo et al. 2015). The inferred timing of the growth and increased migration of L2 (~ca. 13th century) is close to the well documented incursion of *Yersinia pestis* from Central Asia into Europe that resulted in explosive plague epidemics (Benedictow 2004). The experience with plague suggests that patterns of connectivity among humans and other disease vectors were shifting at this place and time, which would potentially open new niches for pathogens including *M.tb*.

We estimate that L1 underwent expansion ~ca. 17th century (fig. 3) but in this case it appears to have grown *in situ*, e.g. due to changing environmental conditions such as increased crowding, and/or growth of local human populations. A study of the molecular epidemiology of TB in Vietnam identified numerous recent migrations of L2 and L4 into the region, versus a stable presence of L1 (Holt et al. 2018); this is consistent with our finding of higher recent rates of migration for L2 and L4 versus L1 (fig. 3). A pattern similar to L1 has been identified previously, in the delay between dispersal of *M.tb* from European migrants to Canadian First Nations and later epidemics of TB driven by shifting disease ecology (Pepperell et al. 2011). These results demonstrate the complex relationship between *M.tb* population growth and migration, and show that under favorable conditions the pathogen can expand into novel niches or accommodate growth in an existing niche.

In a previous study, we used analyses of synonymous and non-synonymous SFS to delineate effects of purifying selection, linkage of sites, and population expansion on global populations of *M.tb* (Pepperell et al. 2013). Simulation studies have shown that purifying selection can affect demographic inference with BEAST and SFS-based methods (Ewing and Jensen 2015; Lapierre et al. 2016). Although our analyses here using ∂a∂i were restricted to synonymous SFS, it is likely that inference of population size changes with this method and with BEAST were affected by purifying selection on this fully linked genome. The magnitude of inferred expansions may thus reflect both population size changes and background selection, and should not be interpreted as direct reflections of historical changes in census population size. We did not detect an effect of purifying selection on inference of migration in our three population simulation analyses (fig. S16, fig. S17), but differences in the strength of purifying selection could contribute to the lineage-specific differences we observed in the size of inferred population expansions: i.e., genome-wide patterns of purifying selection could differ among lineages. We previously found evidence suggesting that the fitness trade-offs of drug resistance mutations vary among lineages (Mortimer et al. 2018), making this intriguing possibility potentially feasible.

While this study comprises the largest phylogeographic analysis on *M.tb* done to date, with 552 isolates collected from 51 countries and all seven described lineages represented, it has some important limitations. We did not attempt to estimate the rate or timescale of *M.tb* evolution, instead relying on published rates that were calibrated with ancient DNA. This is an active area

of research, and newly discovered ancient *M.tb* DNA samples will likely refine inference of both the timing and locations of historical migration events, though it is critical to note that recent substitution rate estimates of *M.tb* have converged on rates around $5x10^{-8}$ substitutions per site per year (Eldholm et al. 2016). Even when substitution rate estimates can be estimated with confidence, the precision with which individual events can be dated using genetic data should not be over-stated, as evidenced by broad 95% credible intervals for internal node date estimates (e.g., Eldholm et al. 2016). Our goal here was to reconstruct historical migration of *M.tb* throughout Eurasia and Africa and place this evolutionary history within a broad historical context; the historical phenomena that we connect with the spread of TB involved vast areas and extended over hundreds and in some cases thousands of years. Our reconstruction of the global dispersal of TB within a temporal framework provided by ancient *M.tb* DNA analysis links spread of the disease to the first ~1500y of the common era, a period of remarkable intensification in the connectedness among peoples of Africa, Asia and Europe (Green 2018).

Methods

Lineage Frequencies. The SITVIT WEB database (Demay et al. 2012), which is an open access *M.tb* molecular markers database, was accessed on September 5, 2016. Spoligotypes were translated to lineages based on the following study (Shabbeer et al. 2012). The following conversions were also included: EAI7-BGD2 for L1, CAS for L3, and LAM7-TUR, LAM12-Madrid1, T5, T3-OSA, and H4 for L4. Isolates containing ambiguous spoligotypes (denoted with >1 spoligotype) were inspected manually and assigned to appropriate lineages. Relative lineage frequencies of lineages 1-6 for each country containing data for >10 isolates were calculated and plotted with the rworldmap package in R (South 2016).

Sample Description.

Old World collection. We assembled/aligned publicly available whole genome sequences (WGS) of thousands of *M.tb* isolates from recently published studies and databases for which country of origin information were known and corresponded to traditional definitions of the Old World. Isolates were assembled via reference guided assembly (RGA) when FASTQ data were available and by multiple genome alignment (MGA) when only draft genome assemblies were accessible (see below). As we were interested in reconstructing historical migrations of the pathogen, we excluded countries where the majority of contemporary TB cases are identified in recent immigrants (Barry et al. 2012; CCDIC 2014; ESR 2015; CDC 2016; PHE 2016; White et al. 2017). Due to computational limitations (BEAST analyses), we necessarily took measures to

limit our dataset to <600 isolates. For countries with large numbers of available genomes, we implemented a sub-sampling strategy similar one previously described (Thorpe et al. 2017), whereby phylogenetic lineage diversity was captured thus minimizing the overrepresentation of clonal complexes (e.g., outbreaks): phylogenetic inference on all isolates available from a country was performed with Fasttree (Price et al. 2010) and a random isolate was selected from each clade extending from *n* branches, where *n* was the desired number of isolates from the country. Numbers of isolates per country were selected based on the availability of appropriate genome sequence data as well as relative TB prevalence (fig. S1) (WHO 2017). All isolates belonging to lineages 5-7 were retained. As a whole, this dataset reflects a 'mixed' sampling scheme (Lapierre et al. 2016), where lineages L5-L7 are overrepresented relative to their contemporary frequencies (fig. 1). At the lineage-specific scale, L1-L4 approximate random sampling of available genomes. Our final Old World collection consisted of the WGS of 552 previously published *M.tb* isolates collected from 51 countries spanning 13 UN geoscheme subregions. Accession numbers and pertinent information about each sample can be found in table S1.

We note that our sample necessarily contains a large number of drug-resistant isolates as these are more commonly sequenced. We also acknowledge that the studies we draw genomes from may have been subject to other sampling biases for which we are unaware.

Northern and Central American collection. For one analysis, we included an additional 15 isolates from a previous study (Comas et al. 2015) for which country of origin information were known and corresponded to the Americas. Isolates were assembled via RGA (see below) and their genotypes at the 3,838,249 bp considered for all analyses of the Old World collection were extracted.

Reference Guided Assembly. Previously published FASTQ data were retrieved from the National Center for Biotechnology Information (NCBI) sequence read archive (SRA) (Leinonen et al. 2011). Low-quality bases were trimmed using a threshold quality of 15, and reads resulting in less than 20bp length were discarded using Trim Galore! (http://www.bioinformatics.babraham.ac.uk/projects/trim_galore/), which is a wrapper tool around Cutadapt (Martin 2011) and FastQC (http://www.bioinformatics.babraham.ac.uk/projects/fastqc/). Reads were mapped to H37Rv (NC_000962.3) (Cole et al. 1998) with the MEM algorithm (Li 2013). Duplicates were removed

using Picard Tools (http://picard.sourceforge.net), and local realignment was performed with GATK (DePristo et al. 2011). To ensure only high quality sequencing data were included, individual sequencing runs for which <80% of the H37Rv genome was covered by at least 20X coverage were discarded, as were runs for which <70% of the reads mapped as determined by Qualimap (García-Alcalde et al. 2012). Pilon (Walker et al. 2014) was used to call variants with the following parameters: --variant --mindepth 10 --minmq 40 --minqual 20.

Multiple Genome Alignment. Draft genome assemblies were aligned to H37Rv (NC_000962.3) (Cole et al. 1998) with Mugsy v1.2.3 (Angiuoli and Salzberg 2011). Regions not present in H37Rv were removed and merged with the reference-guided assembly.

SNP alignment. Variant calls (VCFs) were converted to FASTAs with in-house scripts that treat ambiguous calls and deletions as missing data (available at https://github.com/pepperell-lab/RGAPepPipe). Transposable elements, phage elements, and repetitive families of genes (PE, PPE, and PE-PGRS gene families) that are poorly resolved with short read sequencing were masked to missing data. Isolates with >20% missing sites were excluded from the Old World collection (table S1). Variant positions with respect to H37Rv were extracted with SNP-sites (Page et al. 2016) resulting in 60,818 variant sites. Only sites where at least half of the isolates had confident data (i.e., non-missing) were included in the phylogeographic models and population genetic analyses (60,787 variant sites; 3,838,249 bp). 1.7% of variant sites landed in loci associated with drug resistance (table S5).

Geographic Information. Geographic locations for each of the 552 samples in the Old World collection were obtained from NCBI and/or the respective publications from which the isolates were first described. When precise geographic information was available (e.g., city, province, etc.), coordinates were obtained from www.mapcoordinates.net. When only country level geographic information was found, the 'Create Random Point' tool in ArcGIS 10.3 was used to randomly place each isolate without specific latitude and longitude inside its respective country; inhospitable areas (e.g., deserts and high mountains) and unpopulated areas from each country using 50m data from Natural Earth (http://www.naturalearthdata.com/downloads, accessed February 17, 2016) were excluded as possible coordinates. The 'precision' column of table S1 reflects which method was used.

Trade Route Information. Data for all trade routes active throughout Europe, Africa, and Asia by 1400 CE were compiled from the Old World Trade Routes (OWTRAD) Project (www.ciolek.com/owtrad.html, accessed February 17, 2016). For each route, both node information (trade cities, oases, and caravanserai) and arc information (the routes between nodes) were imported into ArcGIS (fig. 6). *M.tb* isolate locations were also imported as points and the 'Generate Near Table' tool was used to assign each isolate to its nearest node in the trade network and is listed in the 'NearPost' column of table S1.

Maximum Likelihood Inference. We used RAxML v8.2.3 (Stamatakis 2014) for maximum likelihood phylogenetic analysis of the Old World collection (all sites where at least half of isolates had non-missing data) under the general time reversible model of nucleotide substitution with a gamma distribution to account for site-specific rate heterogeneity. Rapid bootstrapping of the corresponding SNP alignment was performed with the -autoMR flag, converging after 50 replicates. Tree visualization was created with the ggtree package in R (Yu et al. 2017).

Structure Analyses. Unsupervised clustering analysis of Old World isolates was performed with STRUCTURE v2.3.4 (Pritchard et al. 2000). For *K* values between 2-12, ten replicate runs consisting of 10,000 burn-in iterations followed by 50,000 iterations were performed with default settings on a subset of the Old World SNP alignment (4053 SNPs occurring at a minor allele frequency > 0.01 with no missing data). StructureHarvester (Earl and vonHoldt 2012) was used to collate results and determine the most suitable value of *K* following the "Evanno" method (Evanno et al. 2005). Replicate runs with the lowest log likelihood for each value of *K* were used for visualization of results.

Phylogeographic & Demographic Inference with BEAST. The Old World collection SNP alignment and individual lineage SNP alignments were analyzed using the Bayesian Markov Chain Monte Carlo coalescent method implemented in BEAST v1.8 (Drummond and Rambaut 2007) with the BEAGLE library (Ayres et al. 2012) to facilitate rapid likelihood calculations. Analyses were performed using the general time reversible model of nucleotide substitution with a gamma distribution to account for rate heterogeneity between sites, a strict molecular clock, and both constant and Bayesian skyline plot (BSP) demographic models. Country of origin or the UN subregion for each isolate was modeled as a discrete phylogenetic trait (Lemey et al. 2009). All Markov chains were run for at least 100 million generations, sampled every 10,000

generations, and with the first 10,000,000 generations discarded as burn-in; replicate runs were performed for analyses and combined to assess convergence. Estimated sample size (ESS) values of non-nuisance parameters were >200 for all analyses. Site and substitution model choice were based on previous analyses of *M.tb* global alignments as opposed to an exhaustive comparison of models which would require unreasonable computational resources. Strict vs relaxed molecular clocks did not result in altered trends of migration at the lineage level, and comparisons between analyses using strict and relaxed clocks show strong correlation between the estimated height of nodes (e.g., $R^2 > 0.97$; fig S18). Table S6 provides a summary of BEAST analyses presented and the results derived from them. Tree visualizations were created with FigTree (http://tree.bio.edu.ac.uk/software/figtree/) and the ggtree package in R (Yu et al. 2017).

We note that phylogeographic inference methods are an active area of research and increasingly sophisticated models are continuously being developed [e.g. (Lemey et al. 2010; De Maio et al. 2015)]. We found alternative methods unsuitable and/or intractable for our large dataset. As methods improve, comparison of the results inferred herein to other phylogeographic models will be important to investigate the sensitivity of our results to the method of phylogeographic inference.

Demographic inference from the observed site frequency spectrum (SFS). SNP-sites (Page et al. 2016) was used to convert the Old World collection alignment to a multi-sample VCF and SnpEff (Cingolani et al. 2012) was used to annotate variants with respect to H37Rv (NC_000962.3) (Cole et al. 1998) as synonymous, non-synonymous, or intergenic. Loci at which any sequence in the population had a gap or unknown character were removed from the data set. Demographic inference with the synonymous SFS for each of the seven lineages and the entire collection was performed using ∂a∂i (Gutenkunst et al. 2009). We modeled constant population size (standard neutral model), an instantaneous expansion model, and an exponential growth model, and identified the best-fit model and maximal likelihood parameters of the demographic model given our observed data. Our parameter estimates, ν and τ, were optimized for the instantaneous expansion and exponential growth models. Uncertainty analysis of these parameters were analyzed using the Godambe Information Matrix (Coffman et al. 2016) on 100 samplings of the observed synonymous SFS with replacement and subsequent model inference.

Population genetic statistics. Nucleotide diversity (π) and Watterson's theta (θ) for various population assignments (e.g., lineage, UN subregion) were calculated with EggLib v2.1.10 (De Mita and Siol 2012).

Analysis of Molecular Variance (AMOVA). AMOVAs were performed using the 'poppr.amova' function (a wrapper for the ade4 package (Dray et al. 2007) implementation) in the poppr package in R (Kamvar et al. 2014). Bins were assigned via the following classification systems: UN geoscheme subregions and Level 1 ('botanical continents') of the World geographical scheme for recording plant distributions. Isolate assignation can be found in table S1. Genetic distances between isolates were calculated with the 'dist.dna' function of the ape v4.0 package in R (Paradis et al. 2004) from the SNP alignment of the Old World collection.

Mantel tests. Great circle distances between *M.tb* isolate locations were calculated with the 'distVincentyEllipsoid' function in the geosphere R package (Hijmans et al. 2016). Geographic distances between isolate locations along the trade network were calculated by adding the great circle distances from the isolates to the nearest trade hubs and the shortest distance between trade hubs along the trade network; the latter was determined using an Origin-Destination Cost Matrix and the 'Solve' tool in the Network Analyst Toolbox of ArcGIS which calculates the shortest distance from each origin to every destination along the arcs in the trade network. In the event that two isolates were assigned to the same trade post, the great circle distance between the isolates was used. To calculate the geographic distance between isolates in a manner that reflects human migrations, the great circle distance between isolates and waypoints were summed. These were calculated with a custom R function (available at https://github.com/ONeillMB1/Mtb_Phylogeography_v2) using a series of rules to define whether or not the path between isolates would have gone through a waypoint. For all three distance metrics, values were log transformed and standardized. Genetic distances between isolates were calculated with the 'dist.dna' function in the ape v4.0 package in R (Paradis et al. 2004) from the SNP alignment. The 'mantel' function of the vegan package in R (Oksanen et al. 2017) was used to perform a Mantel test between the genetic distance matrix and each of the three geographic matrices for both the Old World collection and each individual lineage. Four of the 552 isolates were excluded from these analyses as they were from Kiribati and trade networks spanning this region were not compiled.

Relationship between genetic diversity and geographic distance from Addis Ababa. For this analysis, we added Northern and Central American datasets, assembled in an identical manner to those of the Old World collection and masked at sites where less than half of the Old World collection had confident data (3,838,249 bp). For each UN subregion, the mean latitude and longitude coordinates for all *M.tb* isolates within the region were calculated. The great circle distances from these average estimates for regions to Addis Ababa were then calculated, using waypoints for between-continent distance estimates to make them more reflective of presumed human migration patterns (Ramachandran et al. 2005). Cairo was used as a waypoint for Eastern Europe, Central Asia, Western Asia, Southern Asia, Eastern Asia, and South Eastern Asia; Cairo and Istanbul were used as waypoints for Western Europe and Southern Europe; Cairo, Anadyr, and Prince Rupert were used as waypoints for Northern and Central America. The distance between each region and Addis Ababa were the sum of the great circle distances between the two points (the average coordinates for the UN subregion and Addis Ababa) and the waypoint(s) in the path connecting them, plus the great circle distance(s) between waypoints if two were used. Treating each UN subregion as a population, the relationship between genetic diversity (assessed with π) and geographic distance from Addis Ababa were explored with linear regression for both the entire Old World collection and individual lineages in R (R Development Core Team). Code is available at https://github.com/ONeillMB1/Mtb_Phylogeography_v2.

Migration Rate Inference. Migration rates through time were inferred from the Bayesian maximum clade credibility trees for the entire Old World collection of *M.tb* isolates (n = 552). Individual lineages that contain isolates from multiple UN subregions (i.e., L1: n = 89, L2: n = 181, L3: n = *65*, and L4: n = 143) were extracted and plotted separately. Only nodes with posterior probabilities greater than or equal to 80% were considered. A migration event was classified as a change in the most probable reconstructed ancestral geographic region from a parent to child node. Median heights of the parent and child nodes were treated as a range of time that the migration event could have occurred. The rate of migration through time for each lineage or the Old World collection was inferred by summing the number of migration events occurring across every year of the time-scaled phylogeny, divided by the total number of branches in existence during each year of the time-scaled phylogeny (both those displaying a migration event and those that do not). Code for these analyses is available at https://github.com/ONeillMB1/Mtb_Phylogeography_v2.

Additionally, relative migration rates between UN subregions were derived from the BEAST analyses of phylogeography. The Bayesian stochastic search variable selection method (BSSVS) for identifying the most parsimonious migration matrix implemented in BEAST as part of the discrete phylogeographic migration model (Lemey et al. 2009) allowed us to use Bayes factors (BF) to identify the migration rates with the greatest posterior support and provide posterior estimates for their relative rates. Strongly supported relative rates (BF > 5) and connectivity among subregions were visualized with Cytoscape v3.2.0 (Shannon et al. 2003) and superimposed onto a map generated with the 'rworldmap' package in R (South 2016). To assess the effect of sampling on migration rate inference, UN regions harboring greater than 10 and 20 isolates were randomly subsampled to even numbers and subject to the same analysis. This was done 10 times each for $n = 10$ and $n = 20$.

Effect of selection on estimates of migration. We performed demographic forward-in-time simulations using the SFS_CODE package (Hernandez 2008), which allows for demographic models with arbitrarily complex migration and selection regimes. Our simulations were performed under a simple two population model or with a more complex three population model. In all simulations, N_e for each population was 1000, θ was 0.001 (O'Neill et al. 2015), and migration between each pair of populations was symmetrical. As there is substantial evidence for little to no recombination in the *M.tb* genome, our simulations were performed without recombination.

The two population simulations were performed under three scenarios: 1) no migration between populations after initial divergence; 2) constant migration after divergence (per generation $M = 0.5$) without selection; and 3) constant migration ($M = 0.5$) with purifying selection (25% of alleles of each population have a population selection coefficient of -1.0, and the rest are neutral) after divergence.

The three population simulations were performed under five scenarios: 1) no migration between populations after simultaneous divergence of the three populations; 2) constant, symmetrical migration after divergence (per generation $M = 0.5$ for all population pairs) without selection; 3) constant, symmetrical migration ($M = 0.5$) with purifying selection (25% of alleles in all populations have a population selection coefficient of -1.0, and the rest are neutral); 4) constant, asymmetrical migration after divergence ($M = 0.5$ for migration between pop0 and pop1, $M = 5.0$ for migration between pop1 and pop2, and $M = 0$ for migration between pop0 and pop2) without

748 selection; and 5) constant, asymmetrical migration after divergence (*M* = 0.5 between pop0 and
749 pop1, *M* = 5.0 between pop1 and pop2, and *M* = 0 between pop0 and pop2) with purifying
750 selection (25% of alleles in all populations have a population selection coefficient of -1.0, and
751 the rest are neutral).
752
753 For all simulations, 25 samples were taken from each population, and sequences of 100000
754 bases were generated. Twenty simulations were performed under each scenario for both the 2
755 population (60 simulations) and 3 population (100 simulations) models. Each sequence
756 alignment was subsequently subjected to migration analysis in ∂a∂i (Gutenkunst et al. 2009, see
757 Note S2) and BEAST v1.8.4 (Drummond and Rambaut 2007). For each Bayesian coalescent
758 analysis, the HKY+G substitution model, a constant population model, and a strict molecular
759 clock model were used. A discrete symmetrical migration model (Lemey et al. 2009) was used
760 to determine migration rates, and BSSVS (Lemey et al. 2009) was used to estimate BF support
761 for migration rates in the 3 population simulations. All Markov chains were run for 10 million
762 generations or until convergence, with samples taken every 10,000 steps, and 10% discarded
763 as burn-in. The package SpreaD3 v0.96 (Bielejec et al. 2016) was used to calculate BF support
764 for migration rates.
765
766 Acknowledgments
767 We would like to thank past and present members of the Pepperell Lab for helpful feedback on
768 the project, and particularly highlight Trent Prall for his contribution to preliminary research on
769 historic human trade routes. We also wish to thank Lucy Weinert for her advice on Mantel test
770 standardization. MBO is supported by the National Science Foundation Graduate Research
771 Fellowship Program (DGE-1255259). CSP is supported by National Institutes of Health
772 (R01AI113287).

References

Alam M, Subrahmanyam S. 2009. Indo-Persian travels in the age of discoveries, 1400-1800. Digit. pr. Cambridge: Cambridge University Press.

André J, Filliozat J. 1986. L'Inde vue de Rome: textes latins de l'antiquité, relatifs à l'Inde. Paris: Belles Lettres.

Angiuoli SV, Salzberg SL. 2011. Mugsy: fast multiple alignment of closely related whole genomes. Bioinformatics 27:334–342.

Ayres DL, Darling A, Zwickl DJ, Beerli P, Holder MT, Lewis PO, Huelsenbeck JP, Ronquist F, Swofford DL, Cummings MP, et al. 2012. BEAGLE: An Application Programming Interface and High-Performance Computing Library for Statistical Phylogenetics. Syst. Biol. 61:170–173.

Ball W. 2016. Rome in the East: The Transformation of an Empire. 2nd ed. London & New York: Routledge.

Barry C, Waring J, Stapledon R, Konstantinos A. 2012. Tuberculosis notifications in Australia, 2008 and 2009. Communicable Diseases Intelligence 36:86-94.

Begley V, De Puma RD. 1991. Rome and India: The Ancient Sea Trade. Madison: University of Wisconsin Press.

Behr MA, Wilson MA, Gill WP, Salamon H, Schoolnik GK, Rane S, Small PM. 1999. Comparative genomics of BCG vaccines by whole-genome DNA microarray. Science 284:1520–1523.

Benedictow OJ. 2004. The Black Death, 1346-1353: the complete history. Woodbridge, Suffolk, UK□; Rochester, N.Y., USA: Boydell Press.

Bielejec F, Baele G, Rodrigo AG, Suchard MA, Lemey P. 2016. Identifying predictors of time-inhomogeneous viral evolutionary processes. Virus Evol. 2:vew023.

Blench R. 1996. The Ethnographic Evidence for Long-distance Contacts between Oceania and East Africa. In: Reade J, editor. The Indian Ocean in antiquity.

Blouin Y, Hauck Y, Soler C, Fabre M, Vong R, Dehan C, Cazajous G, Massoure P-L, Kraemer P, Jenkins A, et al. 2012. Significance of the Identification in the Horn of Africa of an Exceptionally Deep Branching Mycobacterium tuberculosis Clade. PLOS ONE 7:e52841.

Bos KI, Harkins KM, Herbig A, Coscolla M, Weber N, Comas I, Forrest SA, Bryant JM, Harris SR, Schuenemann VJ, et al. 2014. Pre-Columbian mycobacterial genomes reveal seals as a source of New World human tuberculosis. Nature 514:494–497.

806 Boussac M-F, Salles J-F, France eds. 1995. Athens, Aden, Arikamedu: essays on the
807 interrelations between India, Arabia, and the eastern Mediterranean. New Delhi:
808 Manohar□: Distributed in South Asia by Foundation Books.

809 Brosch R, Gordon SV, Marmiesse M, Brodin P, Buchrieser C, Eiglmeier K, Garnier T, Gutierrez
810 C, Hewinson G, Kremer K, et al. 2002. A new evolutionary scenario for the
811 Mycobacterium tuberculosis complex. Proc. Natl. Acad. Sci. 99:3684–3689.

812 Butcher K. 2003. Roman Syria and the Near East. Los Angeles: J. Paul Getty Museum□: Getty
813 Publications.

814 Centers for Disease Control and Prevention (CDC). 2016. Reported Tuberculosis in the United
815 States, 2015. Atlanta, GA: US Department of Health and Human Services.

816 Centre for Communicable Diseases and Infection Control (CCDIC). 2014. Tuberculosis
817 prevention and control in Canada a federal framework for action. Public Health Agency
818 of Canada.

819 Cingolani P, Platts A, Wang LL, Coon M, Nguyen T, Wang L, Land SJ, Lu X, Ruden DM. 2012.
820 A program for annotating and predicting the effects of single nucleotide polymorphisms,
821 SnpEff. Fly (Austin) 6:80–92.

822 Coffman AJ, Hsieh PH, Gravel S, Gutenkunst RN. 2016. Computationally Efficient Composite
823 Likelihood Statistics for Demographic Inference. Mol. Biol. Evol. 33:591–593.

824 Cole ST, Brosch R, Parkhill J, Garnier T, Churcher C, Harris D, Gordon SV, Eiglmeier K, Gas S,
825 III CEBI, et al. 1998. Erratum: Deciphering the biology of Mycobacterium tuberculosis
826 from the complete genome sequence. Nat. Lond. 396:190.

827 Comas I, Coscolla M, Luo T, Borrell S, Holt KE, Kato-Maeda M, Parkhill J, Malla B, Berg S,
828 Thwaites G, et al. 2013. Out-of-Africa migration and Neolithic coexpansion of
829 Mycobacterium tuberculosis with modern humans. Nat. Genet. 45:1176–1182.

830 Comas I, Hailu E, Kiros T, Bekele S, Mekonnen W, Gumi B, Tschopp R, Ameni G, Hewinson
831 RG, Robertson BD, et al. 2015. Population Genomics of Mycobacterium tuberculosis in
832 Ethiopia Contradicts the Virgin Soil Hypothesis for Human Tuberculosis in Sub-Saharan
833 Africa. Curr. Biol. 25:3260–3266.

834 Coningham R, Young R. 2015. The Archaeology of South Asia: From the Indus to Asoka,
835 c.6500 BCE–200 CE. Cambridge University Press.

836 De Maio N, Wu C-H, O'Reilly KM, Wilson D. 2015. New Routes to Phylogeography: A
837 Bayesian Structured Coalescent Approximation. PLoS Genet 11:e1005421.

838 De Mita S, Siol M. 2012. EggLib: processing, analysis and simulation tools for population
839 genetics and genomics. BMC Genet. 13:27.

840 Demay C, Liens B, Burguière T, Hill V, Couvin D, Millet J, Mokrousov I, Sola C, Zozio T,
841 Rastogi N. 2012. SITVITWEB – A publicly available international multimarker database
842 for studying Mycobacterium tuberculosis genetic diversity and molecular epidemiology.
843 Infect. Genet. Evol. 12:755–766.

844 DePristo MA, Banks E, Poplin R, Garimella KV, Maguire JR, Hartl C, Philippakis AA, del
845 Angel G, Rivas MA, Hanna M, et al. 2011. A framework for variation discovery and
846 genotyping using next-generation DNA sequencing data. Nat. Genet. 43:491–498.

847 Dilke O. 1985. Greek and Roman Maps. Baltimore: Johns Hopkins University Press

848 Dray S, Dufour A-B, others. 2007. The ade4 package: implementing the duality diagram for
849 ecologists. J. Stat. Softw. 22:1–20.

850 Drummond AJ, Rambaut A. 2007. BEAST: Bayesian evolutionary analysis by sampling trees.
851 BMC Evol. Biol. 7:214.

852 Duchêne S, Holt KE, Weill F-X, Le Hello S, Hawkey J, Edwards DJ, Fourment M, Holmes EC.
853 2016. Genome-scale rates of evolutionary change in bacteria. Microb. Genomics 2:
854 e000094.

855 Earl DA, vonHoldt BM. 2012. STRUCTURE HARVESTER: a website and program for
856 visualizing STRUCTURE output and implementing the Evanno method. Conserv. Genet.
857 Resour. 4:359–361.

858 Eldholm V, Balloux F. 2016. Antimicrobial Resistance in Mycobacterium tuberculosis: The Odd
859 One Out. Trends Microbiol. 24:637–648.

860 Eldholm V, Pettersson JH-O, Brynildsrud OB, Kitchen A, Rasmussen EM, Lillebaek T, Rønning
861 JO, Crudu V, Mengshoel AT, Debech N, et al. 2016. Armed conflict and population
862 displacement as drivers of the evolution and dispersal of Mycobacterium tuberculosis.
863 Proc. Natl. Acad. Sci. 113:13881–13886.

864 Erdkamp P. 2002. The Roman Army and the Economy. Amsterdam: Gieben.

865 Evanno G, Regnaut S, Goudet J. 2005. Detecting the number of clusters of individuals using the
866 software structure: a simulation study. Mol. Ecol. 14:2611–2620.

867 Ewing GB, Jensen JD. 2015. The consequences of not accounting for background selection in
868 demographic inference. Mol. Ecol. 25:135–141.

869 Firdessa R, Berg S, Hailu E, Schelling E, Gumi B, Erenso G, Gadisa E, Kiros T, Habtamu M,
870 Hussein J, et al. 2013. Mycobacterial lineages causing pulmonary and extrapulmonary
871 tuberculosis, Ethiopia. Emerg. Infect. Dis. 19:460–463.

872 Gagneux S, DeRiemer K, Van T, Kato-Maeda M, de Jong BC, Narayanan S, Nicol M, Niemann
873 S, Kremer K, Gutierrez MC, et al. 2006. Variable host–pathogen compatibility in
874 Mycobacterium tuberculosis. Proc. Natl. Acad. Sci. U. S. A. 103:2869–2873.

García-Alcalde F, Okonechnikov K, Carbonell J, Cruz LM, Götz S, Tarazona S, Dopazo J, Meyer TF, Conesa A. 2012. Qualimap: evaluating next-generation sequencing alignment data. Bioinformatics 28:2678–2679.

Green MH. 2018. Climate and Disease in Medieval Eurasia. Oxf. Res. Encycl. Asian Hist.

Gutenkunst RN, Hernandez RD, Williamson SH, Bustamante CD. 2009. Inferring the Joint Demographic History of Multiple Populations from Multidimensional SNP Frequency Data. PLoS Genet 5:e1000695.

Hansen V. 2012. The Silk Road: A New History. Oxford: Oxford University Press.

Hernandez RD. 2008. A flexible forward simulator for populations subject to selection and demography. Bioinformatics 24:2786–2787.

Hershberg R, Lipatov M, Small PM, Sheffer H, Niemann S, Homolka S, Roach JC, Kremer K, Petrov DA, Feldman MW, et al. 2008. High functional diversity in Mycobacterium tuberculosis driven by genetic drift and human demography. PLoS Biol. 6:e311.

Hijmans RJ, Williams E, Vennes C. 2016. geosphere: Spherical Trigonometry. Available from: https://cran.r-project.org/web/packages/geosphere/index.html

Hirsh AE, Tsolaki AG, DeRiemer K, Feldman MW, Small PM. 2004. Stable association between strains of Mycobacterium tuberculosis and their human host populations. Proc Natl Acad Sci U A 101:4871–4876.

Holt KE, McAdam P, Thai PVK, Thuong NTT, Ha DTM, Lan NN, Lan NH, Nhu NTQ, Hai HT, Ha VTN, et al. 2018. Frequent transmission of the Mycobacterium tuberculosis Beijing lineage and positive selection for the EsxW Beijing variant in Vietnam. Nat. Genet. 50:849–856.

Institute of Environmental Science and Research Ltd (ESR). 2015. Tuberculosis in New Zealand: Annual Report 2014. Porirua: ESR.

Isaac BH. 2004. The limits of empire: the Roman army in the East. Oxford: Clarendon Press.

Jong D, C B, Hill PC, Aiken A, Awine T, Martin A, Adetifa IM, Jackson-Sillah DJ, Fox A, Kathryn D, et al. 2008. Progression to Active Tuberculosis, but Not Transmission, Varies by Mycobacterium tuberculosis Lineage in The Gambia. J. Infect. Dis. 198:1037–1043.

Kamvar ZN, Tabima JF, Grünwald NJ. 2014. Poppr: an R package for genetic analysis of populations with clonal, partially clonal, and/or sexual reproduction. PeerJ 2:e281.

Kay GL, Sergeant MJ, Zhou Z, Chan JZ-M, Millard A, Quick J, Szikossy I, Pap I, Spigelman M, Loman NJ, et al. 2015. Eighteenth-century genomes show that mixed infections were common at time of peak tuberculosis in Europe. Nat. Commun. 6:6717.

908 Kent RK. 1979. The Possibilities of Indonesian Colonies in Africa with Reference to
909 Madagascar. In: Mouvements de Populations dans L'Ocean Indie. Paris: H. Champion. p.
910 93–105.

911 Lapierre M, Blin C, Lambert A, Achaz G, Rocha EPC. 2016. The Impact of Selection, Gene
912 Conversion, and Biased Sampling on the Assessment of Microbial Demography. Mol.
913 Biol. Evol. 33:1711–1725.

914 Leinonen R, Sugawara H, Shumway M. 2011. The Sequence Read Archive. Nucleic Acids Res.
915 39:D19–D21.

916 Lemey P, Rambaut A, Drummond AJ, Suchard MA. 2009. Bayesian Phylogeography Finds Its
917 Roots. PLOS Comput. Biol. 5:e1000520.

918 Lemey P, Rambaut A, Welch JJ, Suchard MA. 2010. Phylogeography Takes a Relaxed Random
919 Walk in Continuous Space and Time. Mol. Biol. Evol. 27:1877–1885.

920 Li H. 2013. Aligning sequence reads, clone sequences and assembly contigs with BWA-MEM.
921 ArXiv13033997 Q-Bio. Available from: http://arxiv.org/abs/1303.3997

922 Luo T, Comas I, Luo D, Lu B, Wu J, Wei L, Yang C, Liu Q, Gan M, Sun G, et al. 2015.
923 Southern East Asian origin and coexpansion of Mycobacterium tuberculosis Beijing
924 family with Han Chinese. Proc. Natl. Acad. Sci. 112:8136–8141.

925 Luttwak EN. 1976. The grand strategy of the Roman Empire: from the first century A.D. to the
926 third. London: Weidenweld & Nicholson.

927 Martin M. 2011. Cutadapt removes adapter sequences from high-throughput sequencing reads.
928 EMBnet.journal 17:10–12.

929 Millar F. 1993. The Roman Near East, 31 B.C.-A.D. 337. Cambridge, Mass: Harvard University
930 Press.

931 Mortimer TD, Weber AM, Pepperell CS. 2018. Signatures of Selection at Drug Resistance Loci
932 in Mycobacterium tuberculosis. mSystems 3:e00108-17.

933 Oksanen J, Blanchet FG, Friendly M, Kindt R, Legendre P, McGlinn D, Minchin PR, O'Hara
934 RB, Simpson GL, Solymos P, et al. 2017. vegan: Community Ecology Package.
935 Available from: https://cran.r-project.org/web/packages/vegan/index.html

936 O'Neill MB, Mortimer TD, Pepperell CS. 2015. Diversity of Mycobacterium tuberculosis across
937 Evolutionary Scales. PLOS Pathog. 11:e1005257.

938 Page AJ, Taylor B, Delaney AJ, Soares J, Seemann T, Keane JA, Harris SR. 2016. SNP-sites:
939 rapid efficient extraction of SNPs from multi-FASTA alignments. Microbial Genetics 2 .

940 Paradis E, Claude J, Strimmer K. 2004. APE: Analyses of Phylogenetics and Evolution in R
941 language. Bioinformatics 20:289–290.

942 Parkin D, Barnes R eds. 2002. Ships and the development of maritime technology in the Indian
943 Ocean. London: RoutledgeCurzon.

944 Pepperell CS, Casto AM, Kitchen A, Granka JM, Cornejo OE, Holmes EC, Birren B, Galagan J,
945 Feldman MW. 2013. The Role of Selection in Shaping Diversity of Natural M.
946 tuberculosis Populations. PLoS Pathog 9:e1003543.

947 Pepperell CS, Granka JM, Alexander DC, Behr MA, Chui L, Gordon J, Guthrie JL, Jamieson
948 FB, Langlois-Klassen D, Long R, et al. 2011. Dispersal of Mycobacterium tuberculosis
949 via the Canadian fur trade. Proc. Natl. Acad. Sci. 108:6526–6531.

950 Pfister R, Bellinger L. 1945. The Excavations at Dura-Europos. Final Report IV: The Textiles.
951 New Haven: Yale University Press.

952 Price MN, Dehal PS, Arkin AP. 2010. FastTree 2 – Approximately Maximum-Likelihood Trees
953 for Large Alignments. PLOS ONE 5:e9490.

954 Pritchard JK, Stephens M, Donnelly P. 2000. Inference of Population Structure Using Multilocus
955 Genotype Data. Genetics 155:945–959.

956 Public Health England (PHE). 2016. Tuberculosis in England: 2016. London, UK: PHE.

957 R Development Core Team. R: A Language and Environment for Statistical Computing. Vienna,
958 Austria: R Foundation for Statistical Computing Available from: http: //www.R-
959 project.org/

960 Ramachandran S, Deshpande O, Roseman CC, Rosenberg NA, Feldman MW, Cavalli-Sforza
961 LL. 2005. Support from the relationship of genetic and geographic distance in human
962 populations for a serial founder effect originating in Africa. Proc. Natl. Acad. Sci. U. S.
963 A. 102:15942–15947.

964 Rauh NK. 2003. Merchants, sailors and pirates in the Roman world. Stroud: Tempus.

965 Ray HP. 2003. The archaeology of seafaring in ancient South Asia. Cambridge□; New York:
966 Cambridge University Press.

967 Ray HP, Salles J-F, Institute of Southeast Asian Studies, Maison de l'Orient méditerranéen
968 ancien (Lyon F, National Institute of Science, Technology and Development Studies,
969 France, Ambassade (India), Centre for Human Sciences. 1996. Tradition and
970 archaeology: early maritime contacts in the Indian Ocean. New Delhi: Manohar
971 Publishers.

972 Rocha EPC, Smith JM, Hurst LD, Holden MTG, Cooper JE, Smith NH, Feil EJ. 2006.
973 Comparisons of dN/dS are time dependent for closely related bacterial genomes. J.
974 Theor. Biol. 239:226–235.

975 Salles J-F. 1996. Achaemenid and Hellenistic Trade in the Indian Ocean. In: The Indian Ocean in
976 antiquity. p. 251–267.

977 Sartre M. 1991. L'Orient romain: provinces et sociétés provinciales en Méditerranée orientale
978 d'Auguste aux Sévères (31 avant J.-C-235 après J.-C.). Paris: Seuil.

979 Shabbeer A, Cowan LS, Ozcaglar C, Rastogi N, Vandenberg SL, Yener B, Bennett KP. 2012.
980 TB-Lineage: An online tool for classification and analysis of strains of Mycobacterium
981 tuberculosis complex. Infect. Genet. Evol. 12:789–797.

982 Shannon P, Markiel A, Ozier O, Baliga NS, Wang JT, Ramage D, Amin N, Schwikowski B,
983 Ideker T. 2003. Cytoscape: A Software Environment for Integrated Models of
984 Biomolecular Interaction Networks. Genome Res. 13:2498–2504.

985 South A. 2016. rworldmap: Mapping Global Data. Available from: https://cran.r-
986 project.org/web/packages/rworldmap/index.html

987 Stamatakis A. 2014. RAxML version 8: a tool for phylogenetic analysis and post-analysis of
988 large phylogenies. Bioinformatics 30:1312–1313.

989 Thorpe HA, Bayliss SC, Hurst LD, Feil EJ. 2017. Comparative Analyses of Selection Operating
990 on Nontranslated Intergenic Regions of Diverse Bacterial Species. Genetics 206:363–
991 376.

992 Vogt B. 1996. Bronze Age Maritime Trade in the Indian Ocean: Harappan Traits on the Oman
993 Peninsula. In: Reade J, editor. The Indian Ocean in antiquity. p. 107–132.

994 Walker BJ, Abeel T, Shea T, Priest M, Abouelliel A, Sakthikumar S, Cuomo CA, Zeng Q,
995 Wortman J, Young SK, et al. 2014. Pilon: An Integrated Tool for Comprehensive
996 Microbial Variant Detection and Genome Assembly Improvement. PLOS ONE
997 9:e112963.

998 White Z, Painter J, Douglas P, Abubakar I, Njoo H, Archibald C, Halverson J, Robson J, Posey
999 DL. 2017. Immigrant Arrival and Tuberculosis among Large Immigrant- and Refugee-
1000 Receiving Countries, 2005-2009. Tuberc. Res. Treat 2017.

1001 Wink A. 2002. From the Mediterranean to the Indian Ocean: Medieval History in Geographic
1002 Perspective. Comp. Stud. Soc. Hist. 44:416–445.

1003 World Health Organization (WHO). 2017. Global tuberculosis report 2017. Geneva: WHO.

1004 Yu G, Smith DK, Zhu H, Guan Y, Lam TT-Y. 2017. ggtree: an r package for visualization and
1005 annotation of phylogenetic trees with their covariates and other associated data. Methods
1006 Ecol. Evol. 8:28–36.

1007 Zarins J. 1996. Obsidian in the Larger Context of Predynastic/Archaic Egyptian Red Sea Trade.
1008 In: Reade J, editor. The Indian Ocean in antiquity. p. 107–132.

Figures and Tables

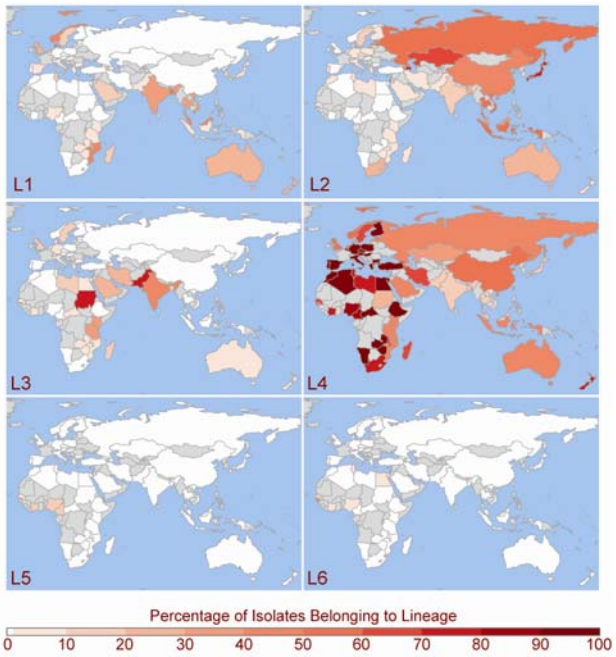

Fig. 1. Geographic distributions of *Mycobacterium tuberculosis* lineages 1-6. Spoligotypes from the SITVIT WEB database (*n* = 42,358) were assigned to lineages 1-6. Countries are colored from white to dark-red based on the percentage of isolates from the country belonging to each lineage. Unsampled countries and those with less than 10 isolates in the database are shown in gray. Lineage 7 (not pictured) is found exclusively in Ethiopia.

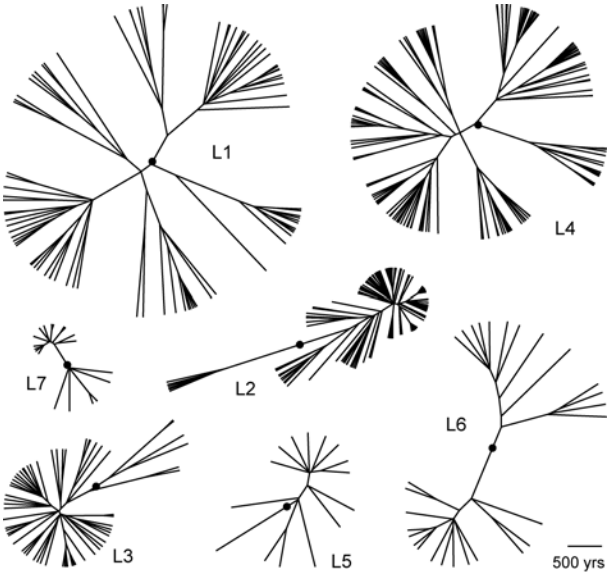

Fig. 2. Maximum clade credibility phylogenies of *Mycobacterium tuberculosis* lineages 1-6. Bayesian analyses were performed on each lineage alignment with the general time reversible model of nucleotide substitution with a gamma distribution to account for rate heterogeneity between sites, a strict molecular clock, and Bayesian skyline plot demographic models. The most recent common ancestor (MRCA) of each lineage is indicated with a black circle; the MRCA of individual lineage phylogenies were informed by the phylogeny of the entire Old World collection, which was dated using a substitution rate of 5×10^{-8} substitutions/site/year (Kay et al. 2015).

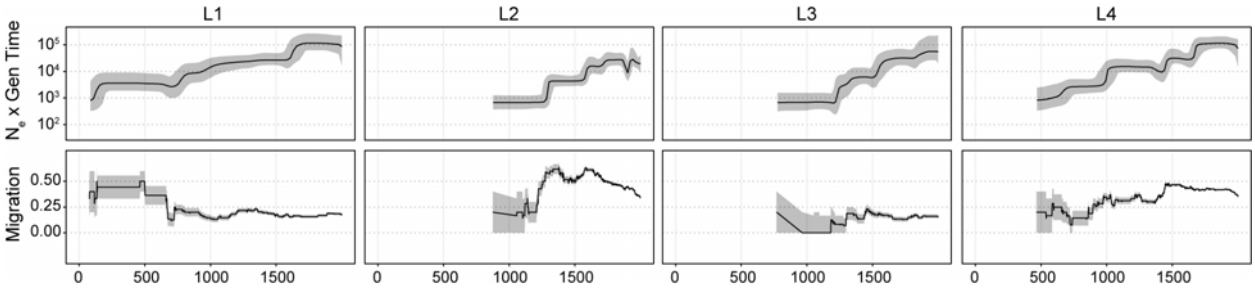

Fig. 3. Patterns of effective population size and migration through time of *Mycobacterium tuberculosis* lineages 1-4. Bayesian skyline plots (top panels) show inferred changes in effective population size (N_e) through time deduced from lineage specific analyses. Black lines denote median N_e and gray shading the 95% highest posterior density. Estimated migration through time (see *Methods*) for each lineage is shown in the bottom panels. Gray shading depicts the rates inferred after the addition or subtraction of a single migration event, and demonstrate the uncertainty of rate estimates, particularly from the early history of each lineage. Dates are shown in calendar years and are based on scaling the phylogeny of the Old World collection with a substitution rate of 5×10^{-8} substitutions/site/year (Kay et al. 2015).

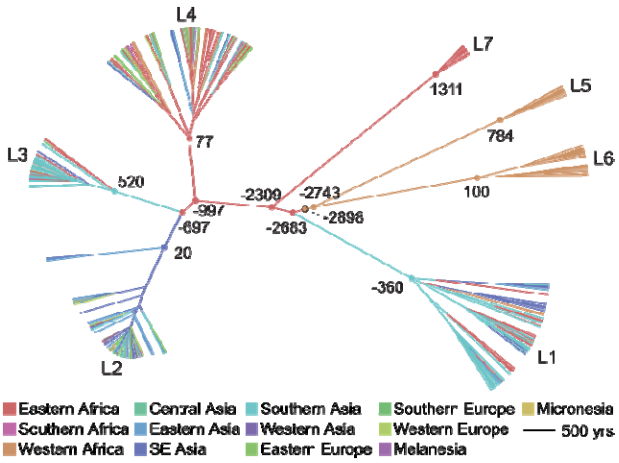

Fig. 4. Maximum clade credibility tree of the Old World collection. Estimated divergence dates are shown in calendar years based on median heights and a substitution rate of 5×10^{-8} substitutions/site/year (Kay et al. 2015). Branches are colored according to the inferred most probable geographic origin. Nodes corresponding to the most recent common ancestors (MRCA) of each lineage, lineage splits, and the MRCA of *M. tuberculosis* (outlined black) are marked with circles and colored to reflect their most probable geographic origin.

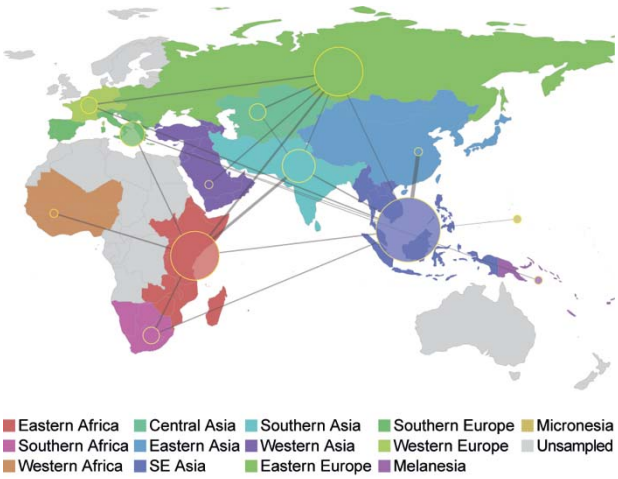

Fig. 5. Connectivity of UN subregions during dispersal of *Mycobacterium tuberculosis*. The Bayesian stochastic search variable selection method was used to identify and quantify migrations with strong support in discrete phylogeographic analysis of the Old World collection. Node sizes reflect the number of significant migrations emanating from the region observed in the phylogeny, whereas the thickness of lines connecting regions reflects the estimated relative rate between regions.

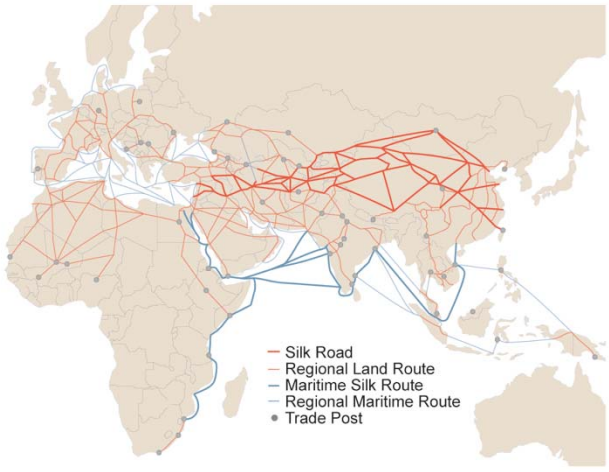

Fig. 6. Trade routes active throughout Europe, Africa and Asia by 1400 CE. Nodes (trade cities, oases, and caravanserai) and arcs (the routes between nodes) are from the Old World Trade Routes Project (www.ciolek.com/owtrad.html, accessed February 17, 2016) and are visualized with ArcGIS.

Table 1. Genetic diversity of Old World *M.tb* across lineages 1-7. TMRCA estimates reflect scaling of results to evolutionary rates calibrated from ancient DNA [median 5.00×10^{-8} substitutions/ site/ year (Kay et al. 2015) and are written as calendar years. To account for uncertainty in this rate estimate, our lower and upper TMRCA estimates reflect scaling of our results with the low and high bounds of the 95% highest posterior density estimates of the rate reported from ancient DNA analysis (i.e. 4.06×10^{-8} and 5.87×10^{-8}, respectively).

		MTBC	***L1***	***L4***	***L2***	***L3***	***L5***	***L6***	***L7***
Sample	***n***	552	89	143	181	65	15	31	28
Diversity	□	2.13E-03	7.56E-04	7.80E-04	4.49E-04	3.88E-04	1.72E-04	3.04E-04	7.99E-05
	π	2.80E-04	1.92E-04	1.54E-04	7.46E-05	9.16E-05	8.77E-05	1.41E-04	4.52E-05
Demographic Inference	***N/Nanc***	91 ± 4	71 ± 5	55 ± 22	112 ± 102	148 ± 2	504 ± 111	50 ± 5	17 ± 4
	Generations (Nanc)	0.16 ± 0.01	0.80 ± 0.06	0.65 ± 0.35	0.41 ± 0.94	3.54 ± 0.04	3.94 ± 0.73	1.10 ± 0.09	2.45 ± 0.89
	LL expansion	-1788.4	-424.2	-492.8	-467.1	-108.2	-42.4	-151.9	-64.5
	LL neutral	-10549.2	-3246.6	-3474.6	-2378.9	-1717.0	-520.7	-912.3	-159.4
	***p*-value**	0.00	0.00	0.00	0.00	0.00	0.00	0.00	0.00
Structure UN subregions	**Var. Between**	21	19	4	20	16	NA	NA	NA
	Var. Within	79	81	96	80	84	NA	NA	NA
	p-value	<0.001	<0.001	0.001	<0.001	0.004	NA	NA	NA
Structure Botanical Continents	**Var. Between**	14	5	2	9	13	NA	NA	NA
	Var. Within	86	95	98	91	87	NA	NA	NA
	p-value	<0.001	0.02	0.05	<0.001	<0.001	NA	NA	NA
TMRCA	**median**	-2898	-360	77	-20	520	784	100	1311
	lower	-4032	-906	-368	-488	177	502	-339	1152
	upper	-2172	-10	362	279	739	964	382	1413
Geographic origin	**1st region**	W Africa	S Asia	E Africa	SE Asia	S Asia	W Africa	W Africa	E Africa
	probability	54.2%	75.6%	98.9%	81.0%	63.5%	99.9%	99.8%	99.8%
	2nd region	E Africa	E Africa	E Europe	E Asia	E Africa	E Africa	E Africa	S Africa
	probability	37.5%	24.1%	0.7%	9.2%	36.2%	0.1%	0.2%	0.0%